J|A|C|S
ARTICLES
Published on Web 02/02/2006

Large Dynamic Stokes Shift of DNA Intercalation Dye Thiazole Orange has Contribution from a High-Frequency Mode

Venugopal Karunakaran, J. Luis Pérez Lustres, Lijuan Zhao,[#]
Nikolaus P. Ernsting,* and Oliver Seitz

Contribution from the Department of Chemistry, Humboldt-Universität zu Berlin, Brook-Taylor-Str. 2, D-12489 Berlin, Germany

Received October 7, 2005; E-mail: nernst@chemie.hu-berlin.de

Abstract: Fluorescence of the cyanine dye Thiazole Orange (TO) is quenched by intramolecular twisting in the excited state. In polypeptide nucleic acids, a vibrational progression in a 1400 cm^{-1} mode depends on base pairing, from which follows that the high-frequency displacement is coupled to the twist coordinate. The coupling is intrinsic to TO. This is shown by femtosecond fluorescence upconversion and transient absorption spectroscopy with the dye in methanol solution. Narrow emission from the Franck−Condon state shifts to the red and broadens within 100 fs. The radiative rate does not decrease during this process. Vibrational structure builds up on a 200 fs time scale; it is assigned to asymmetric stretching activity in the methine bridge. Further Stokes shift and decay are observed over 2 ps. Emission from the global S_1 minimum is discovered in an extremely wide band around 12 000 cm^{-1}. As the structure twists away from the Franck−Condon region, the mode becomes more displaced and overlap with increasingly higher vibrational wave functions of the electronic ground state is achieved. Twisting motion is thus leveraged into a fast-shrinking effective energy gap between the two electronic states, and internal conversion ensues.

1. Introduction

The asymmetric cyanine dye Thiazole Orange (TO, 2-[1-carboxymethyl-1*H*-quinolin-4-ylidenmethyl]-3-methylbenzothiazol-3-ium bromide, Scheme 1) is essentially nonfluorescent in aqueous solution (quantum yield = 0.0002).[1] The visible absorption and fluorescence spectra of TO in methanol are shown in Figure 1. The chromophore is cationic and has high affinity for polynucleic acids, where it intercalates (association constant = 3.3×10^5 M^{-1}).[1] Thus braced with nucleobases, the nonradiative decay channel is closed and the fluorescence yield increases to 0.1−0.4 in double-stranded (ds) DNA.[1] TO and similar cyanine dyes, for example, substituted PicoGreen[2] or the corresponding oxazole,[3] are therefore used to detect and quantify polynucleotides in a variety of techniques.[4−10] Examples include the hybridization of single strands,[8] monitoring the polymerase chain reaction,[9] and capillary electrophoresis.[10]

Scheme 1. Thiazole Orange (TO) in its Most Stable Conformation in the Electronic Ground State[a]

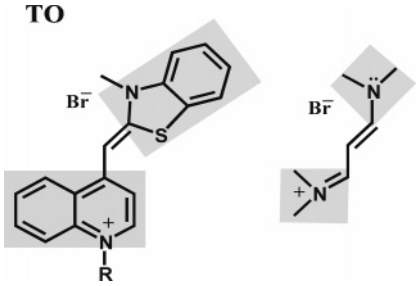

[a] The lowest isomer (10 kcal/mol above, from AM1 calculations) has the thiazolyl group rotated by 180°. The photoreaction of TO involves torsional motion of the two moieties (gray rectangles) around the central methine bridge. Structural changes will be illustrated with a small model cyanine[18,19] (right). For simplicity, only one VB structure is shown in each case.

The affinity toward dsDNA can be increased with positively charged side chains[11] or by linking two chromophores through a tether which carries multiple positive charges.[4] A major issue with intercalation dyes is whether they prefer specific base sequences.[12] Specificity by design was achieved when a TO−peptide conjugate was linked into a single-stranded sequence.[13] Hybridization was possible with every natural base paired against the chromophore, it could be monitored by a 20-fold increase of fluorescence, and the increase is sensitive to the

[#] During leave from the Photonic Research Center, Nankai University, China.

(1) Nygren, J.; Svanvik, N.; Kubista, M. *Biopolymers* **1998**, *46*, 39−51.
(2) Cosa, G.; Focsaneanu, K. S.; McLean, N. R. J.; Scaiano, J. C. *Chem. Commun.* **2000**, 689−690.
(3) Simon, L. D.; Abramo, K. H.; Sell, K. J.; McGown, B. L. *Biospectroscopy* **1998**, *4*, 17−25.
(4) Glazer, A. N.; Rye, S. H. *Nature* **1992**, *359*, 859−861.
(5) Rye, H. S.; Quesada, M. A.; Peck, K.; Mathies, R. A.; Glazer, A. N. *Nucleic Acids Res.* **1991**, *19*, 327−333.
(6) Lee, L. G.; Chen, C. H.; Chiu, L. A. *Cytometry* **1986**, *7*, 508−517.
(7) Srinivasan, K.; Morris, S. C.; Girard, J. E.; Kline, M. C.; Reeder, D. J. *Appl. Theor. Electrophor.* **1993**, *3*, 235−239.
(8) Privat, E.; Melvin, T.; Merola, F.; Schweizer, G.; Prodhomme, S.; Asseline, U.; Vigny, P. *Photochem. Photobiol.* **2002**, *75*, 201−210.
(9) Svanvik, N.; Stählberg, A.; Sehlstedt, U.; Sjöback, R.; Kubista, M. *Anal. Biochem.* **2000**, *287*, 179−182.
(10) Zhu, H.; Clark, S. M.; Benson, S. C; Rye, H. S.; Glazer, A. N.; Mathies, R. A. *Anal. Chem.* **1994**, *66*, 1941−1948.
(11) Petty, T. J.; Bordelon, A. J.; Robertson, E. M. *J. Phys. Chem. B* **2000**, *104*, 7221−7227.
(12) Schweitzer, C.; Scaiano, J. C. *Phys. Chem. Chem. Phys.* **2003**, *5*, 4911−4917.
(13) Köhler, O.; Jarikote, D. V.; Seitz, O. *Chem. Commun.* **2004**, 2674−2675.

10.1021/ja056862n CCC: $33.50

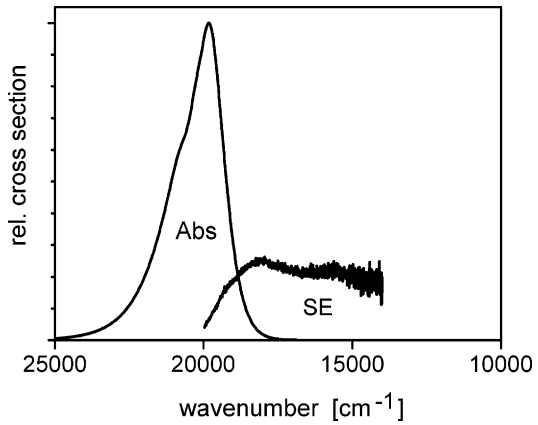

Figure 1. Stationary absorption and emission spectra of TO in methanol. The measured fluorescence quantum distribution (λ_{exc} = 480 nm) was converted into cross-sections for stimulated emission SE; only relative values are given.

mismatch of a neighboring pair.[14] The latter observation suggests that a DNA target may be distinguished from its base mutant by fluorescence directly, and this aim motivated the present study.

The mechanism which governs the interaction of TO with neighboring nucleotides is crucial for applications. It is based on the photochemistry of cyanines in pure solvents, which was studied extensively (see recent examples[15−17] and references therein). Cyanines have two heterocyclic moieties which are coplanar in the electronic ground state, S_0. The intense $S_1(\pi\pi^*) \leftarrow S_0$ absorption band can be tuned from the visible to the near-infrared region by varying the length of the (poly)methine bridge between the ring systems. Optical excitation leads to a region on the S_1 potential-energy hypersurface which is not stable; the two moieties begin to twist around their connecting bonds, and the Franck−Condon (FC) region is left on a 100 fs time scale so that fluorescence is effectively avoided. The structural and electronic changes along the S_1 reaction path were examined recently in computational studies of symmetrical model carbocyanines.[18−20] The results for the trimethine cyanine[18,19] (Scheme 1) are summarized in Figure 2, where δ and ϵ measure the deviation of the bridge dihedral angles from their initial *trans* conformation in the directions shown. Twisting of the moieties against each other is thus described as conrotary, $\delta = \epsilon$, toward the perpendicular conformation at $\delta = 45°$. However, different high-frequency modes are predicted to be active along the way (this is indicated by vibrational parabolas which are oriented in orthogonal directions). Initially, excitation $S_1 \leftarrow S_0$ is accompanied by symmetric expansion of the bridge bonds which continues on the S_1 hypersurface until $\delta \approx 20°$ (process 1). For symmetric cyanines, the positive charge should so far be distributed equally over the two moieties. Then asymmetric distortion sets in, and the positive charge becomes localized. During this process (2), the asymmetric displacement in S_1 increases strongly with twist angle until the perpendicular conformation is reached (note a corresponding displacement "wedge" in the figure). The scheme implies a wide FC progression in a high-frequency mode for fluorescence at large twist angles—provided there is sufficient radiative coupling. Next, while keeping the perpendicular form, the plane of the bridge turns to become coplanar with the charged moiety (described by disrotary motion 3) along a more gentle slope of the S_1 surface, and the global minimum is thus reached. From here, a conical intersection (CI) can be accessed by asymmetric stretching so that internal conversion is an activated process (4), partly to the *cis* isomer and partly back to the original *trans* form.[21] The intersection is accessible at all torsional angles so

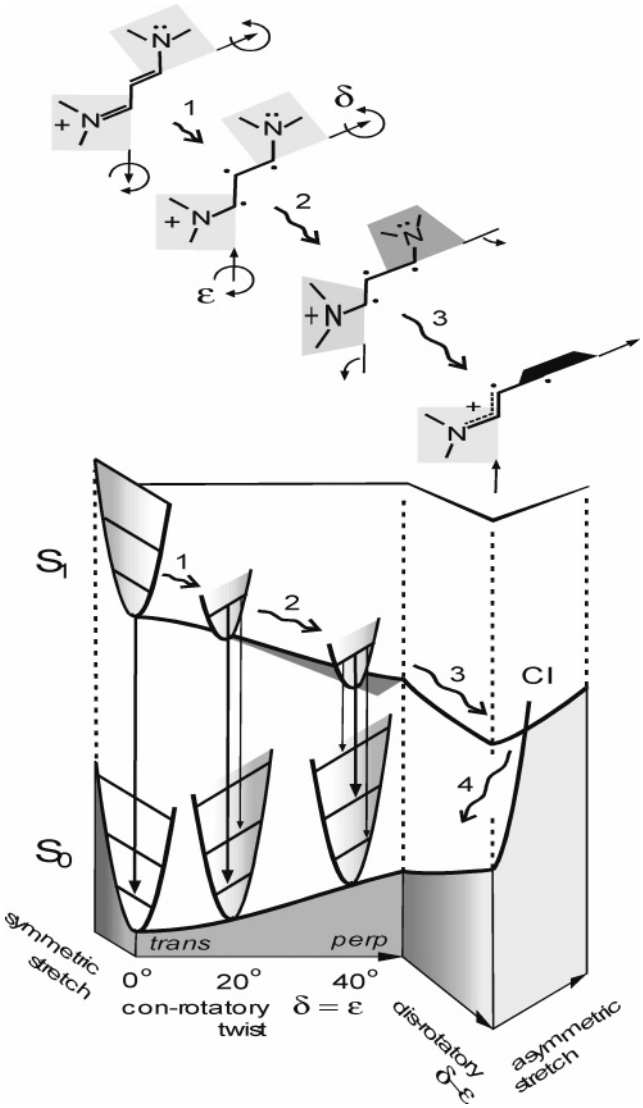

Figure 2. Photoreaction in S_1 as calculated for a symmetric model cyanine,[18] for twist angles δ, ϵ from the all-*trans* conformation of S_0. Optical absorption $S_1 \leftarrow S_0$ initially causes symmetric expansion and conrotary twisting (1) until $\delta = \epsilon \approx 20°$. Then asymmetric distortion sets in, strongly increasing with further conrotation (2), and the positive charge becomes localized. After the perpendicular conformation is reached, the bridge plane turns coplanar with the charged moiety (described by disrotary motion 3). Internal conversion (4) is an activated process involving asymmetric stretching from the global minimum to a conical intersection (CI). In this work, the fluorescence band of Thiazole Orange in methanol is characterized during the entire time in S_1.

(14) Köhler, O.; Seitz, O. *Chem. Commun*. **2003**, 2938−2939.
(15) Huang, Z.; Ji, D.; Xia, A.; Koberling, F.; Patting, M.; Erdmann, R. *J. Am. Chem. Soc*. **2005**, *127*, 8064−8066.
(16) Mishra, A.; Behera, K. R.; Behera, K. P.; Mishra, K. B.; Behera, B. G. *Chem. Rev*. **2000**, *100*, 1973−2011.
(17) (a) Alvarez, J.-L.; Yartsev, A.; Äberg, U.; Äkesson, E.; Sundström, V. *J. Phys. Chem. B* **1998**, *102*, 7651−7658. (b) Yartsev, A.; Alvarez, J.-L.; Åberg, U.; Sundström, V. *Chem. Phys. Lett.* **1995**, *243*, 281−289.
(18) Sanchez-Galvez, A.; Hunt, P.; Robb, A. M.; Olivucci, M.; Vreven, T.; Schlegel, B. H. *J. Am. Chem. Soc*. **2000**, *122*, 2911−2924.
(19) Hunt, P.; Robb, M. A. *J. Am. Chem. Soc.* **2005**, *127*, 5720−5726.
(20) Improta, R.; Santoro, F. *J. Chem. Theor. Comput.* **2005**, *1*, 215−229.
(21) Sundström, A.; Gillbro, T. *J. Phys. Chem*. **1982**, *86*, 1788−1794.

that the S_1 minimum may not be reached at all or at least be of little importance for the dynamics.[19]

Returning to Thiazole Orange, it would be useful to have a similarly detailed view of its potential-energy surface along the reaction path to guide modifications and linkage for DNA sensing, but the molecule is larger than the model compounds studied above and is not easily calculated with comparable accuracy. It also has lower symmetry, and a conical intersection can only be accidental; hence it is unlikely to dominate the dynamics. Instead, we follow an experimental approach to characterize structural changes of TO. A large number of symmetrical cyanines have recently been studied by transient absorption spectroscopy with an emphasis on excited-state absorption $S_n \leftarrow S_1$.[17,22−23] Yet what is most interesting for applications is radiative coupling $S_1 \rightarrow S_0$ during the photoreaction. This is why we aim for a quantitative characterization of the fluorescence spectrum as it evolves after femtosecond optical excitation. For this purpose, transient absorption spectra are recorded over a wide frequency range which covers the emission region to the near-infrared. We also use a novel fluorescence technique which cuts 80 fs slices from the evolving emission and measures the corresponding time-resolved spectra with photometric precision. By combining both sets of data, characteristic transient emission spectra are extracted and related to the model reaction scheme of Figure 2. From narrow FC fluorescence, extended vibrational structure builds up on a 200 fs time scale in methanol. Emission is observed in an extremely wide band around 12 000 cm^{-1}. Its oscillator strength (>0.15) is substantial for a structure considered to be perpendicular (the global S_1 minimum), which needs explaining by computational chemistry.

Let us consider fluorescence enhancement as the dye enters (or is linked into) a polynucleotide. Ideally, the quantum yield should be understood in terms of sequence and base pairing; in the remainder of this section, we show the complexity of that task. The general view on cyanines is that the extent of twisting or torsion between the heterocycle moieties is reduced when near-range interactions are increased.[16] There are two aspects to this effect. In an environment of higher viscosity, the motion is more damped and the process slowed even though the S_1 potential-energy surface may be unaffected. On the other hand, stacked nucleobases on either side impede torsion directly; that is, they bend the S_1 surface upward along the twist coordinate. Hence, after optical excitation, the population remains in the vicinity of the FC point on the S_1 potential-energy surface and emission is observed. Because twisting is admitted to various degrees, different limiting energy gaps should be reached depending on the pairing of neighboring bases, which therefore sensitively influences the fluorescence quantum yield. However, the stationary emission spectrum is also affected in more subtle ways, as can be seen when TO is linked into a peptide nucleic acid (PNA) oligomer[24] and hybridized with various complementary strands.[13,14] Several such constructs and their optical spectra are shown in Figure 3, where the corresponding emission quantum yields are also given. Fluorescence exhibits a progression of three vibrational bands for all constructs, extending to

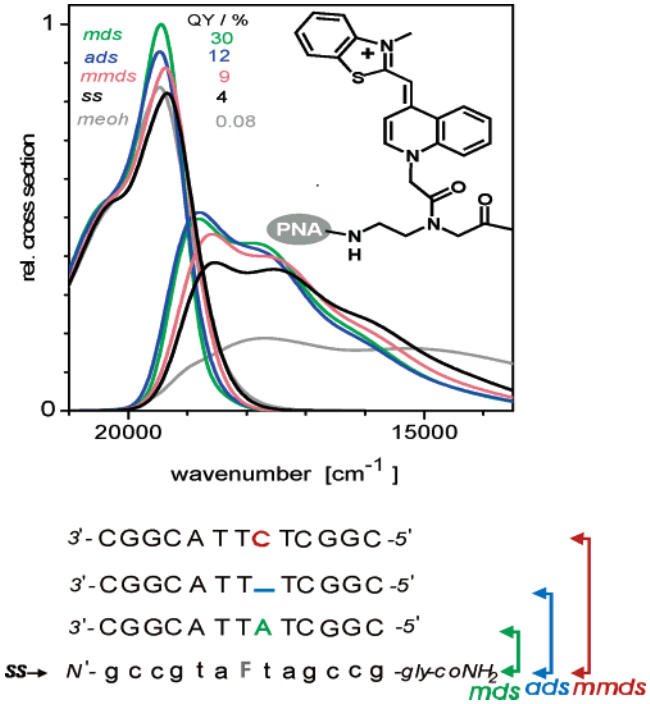

Figure 3. Fluorescence spectrum and quantum yield of TO in polypeptide nucleic acids, in place of a nucleobase, depend on the pairing of neighboring bases.[13] Single-stranded (ss) PNA sequence with fluorophore F; mds = matched, ads = abasic (i.e., without nucleobase opposite), mmds = mismatched double-stranded PNA/DNA. Spectra of TO in methanol are shown for comparison (gray, shifted by −480 cm^{-1}). All spectra normalized to oscillator strength except emission in methanol and smoothed for better comparison.

the red by more than 4000 cm^{-1}. Referring to the reaction path in Figure 2, we may identify the progression with asymmetric stretching of the methine bridge on the conrotary section of the path. The effective mode displacement, *d*, is obviously different for the various constructs, whereas the vibrational frequency is constant. The pertinent parameters may be estimated by a description of the optical spectra through Brownian oscillators,[25] as shown in Figure 4 for TO in single-stranded PNA. The absorption shows an active mode in S_1 at 1350 cm^{-1} with dimensionless displacement, $d \approx 1.11$, from the S_0 geometry. In emission, on the other hand, the active mode in S_0 has an estimated vibrational frequency of 1400 cm^{-1} and needs $d \approx 1.52$ from the S_1 geometry for broad vibronic structure. (Even a small change of *d* causes serious reshaping of the fluorescence spectrum; therefore *d* can be estimated to ±0.02. For a quantitative description, the distribution of *d* along the twist coordinate must be included.) However, displacement and quantum yield are not related in a monotonic fashion, as the model reaction path alone would suggest. For example, by going from *mds* to *ads*, the quantum yield drops from 30 to 12%, while the displacement *decreases* slightly from $d = 1.41$, as can be seen by inspection of Figure 3. This inversion becomes more pronounced when the next nucleobase in the labeled strand (t) is deleted to form an basic site.[26] The observations prove that neighboring nucleobases not only restrict torsional volume but also distort the S_1 potential-energy surface along high-

(22) Meyer, H. Y.; Pittman, M.; Plaza, P. *J. Photochem. Photobiol. A: Chem.* **1998**, *114*, 1−21.
(23) Åberg, U.; Åkesson, E.; Alvarez, J.-L.; Fedchenia, I.; Sundström, V. *Chem. Phys.* **1994**, *183*, 269−288.
(24) Jarikote, D. V.; Köhler, O.; Socher, E.; Seitz. O. *Eur. J. Org. Chem.* **2005**, 3187−3195.
(25) Bosma, B. W.; Yan, J. Y.; Mukamel, S. *Phys. Rev. A* **1990**, *42*, 6920−6923.
(26) Karunakaran, V.; Ernsting, P. N.; Jarikote, V. D.; Seitz, O. Manuscript in preparation.

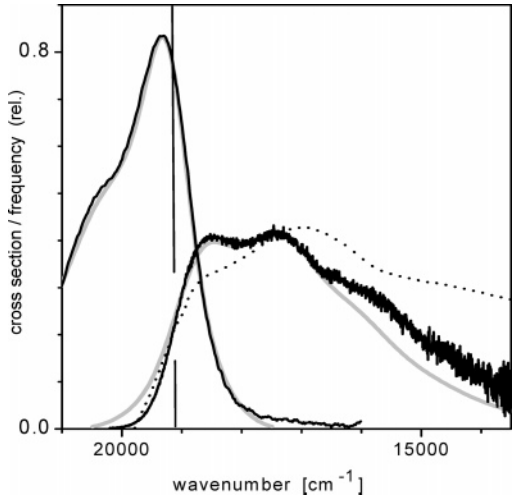

Figure 4. Band shapes of TO in single-stranded PNA (solid lines) described by the Brownian oscillator model[25] (gray). The absorption shows an active mode in S_1 at 1350 cm^{-1} with dimensionless displacement $d \approx 1.11$ from the S_0 geometry. The emission needs $d \approx 1.52$ for broad vibronic structure, and the vibrational frequency is estimated to be 1400 cm^{-1}. Transient absorption in methanol at 300 fs is shown for comparison (spectrum L from Figure 7b shifted by -480 cm^{-1} and scaled; dashed line). The absorption origin is marked by a vertical line.

frequency coordinates. Therefore, to measure *intrinsic* photophysical properties of Thiazole Orange, we focus in this work on the chromophore free in solution.

2. Results

Stationary absorption and emission spectra of Thiazole Orange in methanol are already shown in Figure 1. The $S_1 \leftarrow S_0$ absorption band peaks at 19 990 cm^{-1} ($\epsilon_{max} = 79 \pm 3 \times 10^3$ L mol^{-1} cm^{-1}), and a blue shoulder indicates vibrational activity. The electronic oscillator strength is estimated to be $f_{abs} \approx 0.72$ and the radiative lifetime $\tau_{rad} \approx 6.2$ ns. Fluorescence is usually discussed in terms of the fluorescence quantum distribution (FQD), but with transient absorption one observes the spectrum of cross-sections for stimulated emission (SE) $\sim$FQD($\tilde{\nu}$)/$\tilde{\nu}^2$, which is therefore shown in the figure. The observed emission band does not mirror the absorption spectrum but extends broadly into the red, which is corroborated by time-resolved measurements below. (Mirror symmetry should properly be discussed with line shape functions, $\epsilon(\tilde{\nu})/\tilde{\nu}$ and FQD($\tilde{\nu}$)/$\tilde{\nu}^3$; see for example, Mataga, N.; Kubota, T. *Molecular Interactions and Electronic Spectra*; Marcel Dekker: New York, 1970; eqs 3−41b. The last division by $\tilde{\nu}$ may be omitted for qualitative arguments.)

Transient absorption spectra are shown in Figure 5. The upper panel (a) shows their evolution during the first picosecond after excitation. Positive induced optical density, ΔOD, corresponds to excited-state absorption (ESA), while negative signal indicates bleach (BL) or stimulated emission (SE). For example, consider the transient spectrum at 1 ps: broad SE is observed from 10 000 to 18 000 cm^{-1}, there is no overlap with the absorption region, and the bleach contribution can be quantified by a negatively scaled absorption band. At 50 fs, on the other hand, SE overlaps with the BL band so that the signal is most negative in between. The pump is still present (but at much lower intensity compared to its peak at $t = 0$), and therefore, the transient absorption spectrum at 50 fs also contains a coherent contribution to the

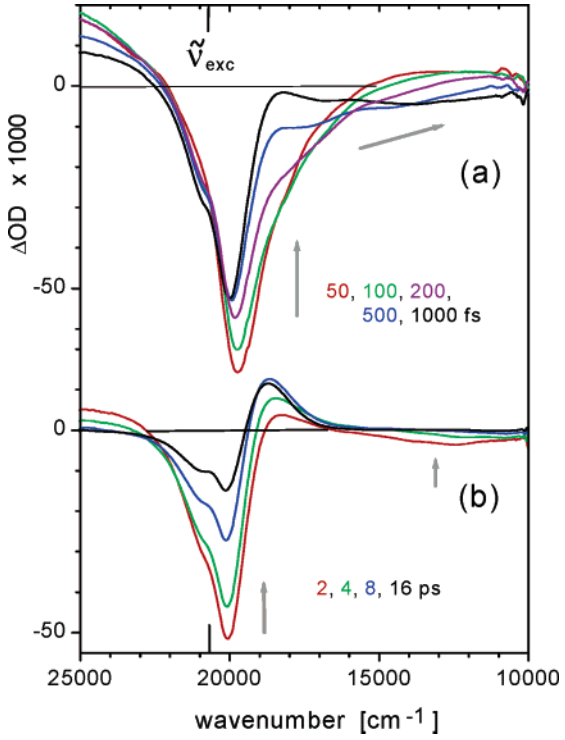

Figure 5. Transient absorption spectra of TO in methanol: (a) subpicosecond time scale showing bleach and red-shift of stimulated emission to the deep red; (b) picosecond scale on which internal conversion and cooling take place. Excitation at 484 nm, 65 fs time resolution fwhm, and magic-angle polarizations.

signal,[27,28] of about $\pm$5 mOD, around the excitation frequency which is centered at 20 690 cm^{-1}.The lower panel (b) covers the time from 2 to 16 ps. During this period, the deep-red emission decays and the transient absorption spectrum gradually assumes a dispersive shape, indicative of a broadened or shifted absorption band. Separate measurements were performed with $\parallel$ and $\perp$ polarization of the pump light relative to that of the supercontinuum. The anisotropy during the first 1.5 ps is 0.36 $\pm$ 0.01 for usable frequencies $\tilde{\nu} \leq 21\,000$ cm^{-1}, that is, in the BL and SE region, and 0.26 $\pm$ 0.01 in the ESA range $\tilde{\nu} \geq 23\,500$ cm^{-1}.

Time-resolved fluorescence spectra of Thiazole Orange are presented in Figure 6 as quantum distributions over frequency.[29] Now overlapping bands from other nonlinear optical processes which complicate transient absorption are absent, and emission from the FC region can be observed directly. For example, at 50 fs the fluorescence band is a mirror image of absorption; the band shifts by 800 cm^{-1} to lower energy during the next 150 fs (compare red and purple lines in Figure 6). Following this initial process, one observes strong broadening toward the red and decay on a subpicosecond time scale. Finally the fluorescence disappears with about 4 ps time constant (not shown).

3. Analysis and Discussion

The analysis begins with the femtosecond fluorescence spectra (Figure 6). For cyanines, the excited-state relaxation involves

(27) Dobryakov, A. L.; Kovalenko, A. S.; Ernsting, *J. Chem. Phys.* **2003**, *119*, 988−1002.
(28) Dobryakov, A. L.; Kovalenko, A. S.; Ernsting, P. N. *J. Chem. Phys.* **2005**, *123*, 044502.
(29) Zhao, L.; Lustres, J. L. P.; Farztdinov, V.; Ernsting, P. N. *Phys. Chem. Chem. Phys.* **2005**, *7*, 1716−1725.

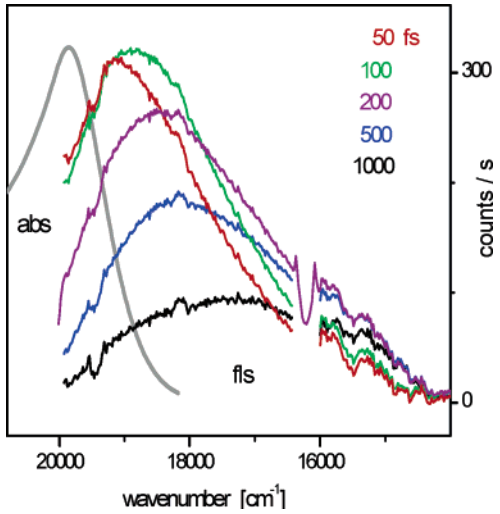

Figure 6. Transient fluorescence spectra of TO in methanol, from broad band upconversion with NIR gate pulses, show an initial red-shift over ~200 fs and subsequent broadening. Excitation at 450 nm, 80 fs time resolution, and parallel polarizations. Signal is expressed as quantum distribution and scaled to the peak count rate. The absorption spectrum is also shown. (An artifact around 16 200 cm^{-1} is due to scatter from the third harmonic of the gate pulse.)

no barrier and consists of continuous downhill motion along twist angles δ, ϵ toward a perpendicular configuration of minimum energy (Figure 2) where internal conversion takes over. We seek characteristic fluorescence spectra along the way which would allow quantitative comparison with their counterparts from transient absorption. For this purpose, the photoreaction is assumed to proceed through virtual states

$$K(S_1) \xrightarrow{k1} L(S_1) \xrightarrow{k2} M(S_1)... \xrightarrow{kj} X(S_0) \xrightarrow{kj+1} Y(S_0)...$$

No physical meaning should be attached a priori to the characteristic intermediates, but of course, internal conversion to S_0 must be sketched in somewhere.

Evidence for internal conversion is (i) the disappearance of emission and (ii) the return to zero of the induced band-integral in transient absorption, as will be shown below. In principle, internal conversion may set in at stage L or earlier so that the kinetic approximation to the dynamics would have to contain a channel, $L(S_1) \rightarrow X(S_0)$. The limitations imposed by our scheme should be kept in mind later. Global analysis of time- and frequency-dependent data was done by singular-value decomposition.[30] For transient fluorescence, we find that the three virtual states, K, L, and M, are necessary and sufficient to describe the spectra and dynamics, with rate constants $k_1 = 4.97$, $k_2 = 1.44$, and $k_3 = 0.21$ ps^{-1}. (A value for k_3 was obtained from transient absorption and kept fixed when fitting the fluorescence evolution. The total analysis was reiterated until consistency was achieved. Other sets of values for k_1-k_3 are also possible. Transient emission spectra were analyzed for $t \geq 150$ fs because $t_0(\tilde{\nu})$ may smoothly deviate in a ±15 fs band around the chosen function and because solvent Raman signal could not be separated from early fluorescence uniquely.) Their time-dependent amplitudes are shown in Figure 7d; these curves describe the relative populations of the three states, convoluted with the apparatus function of the fluorescence experiment

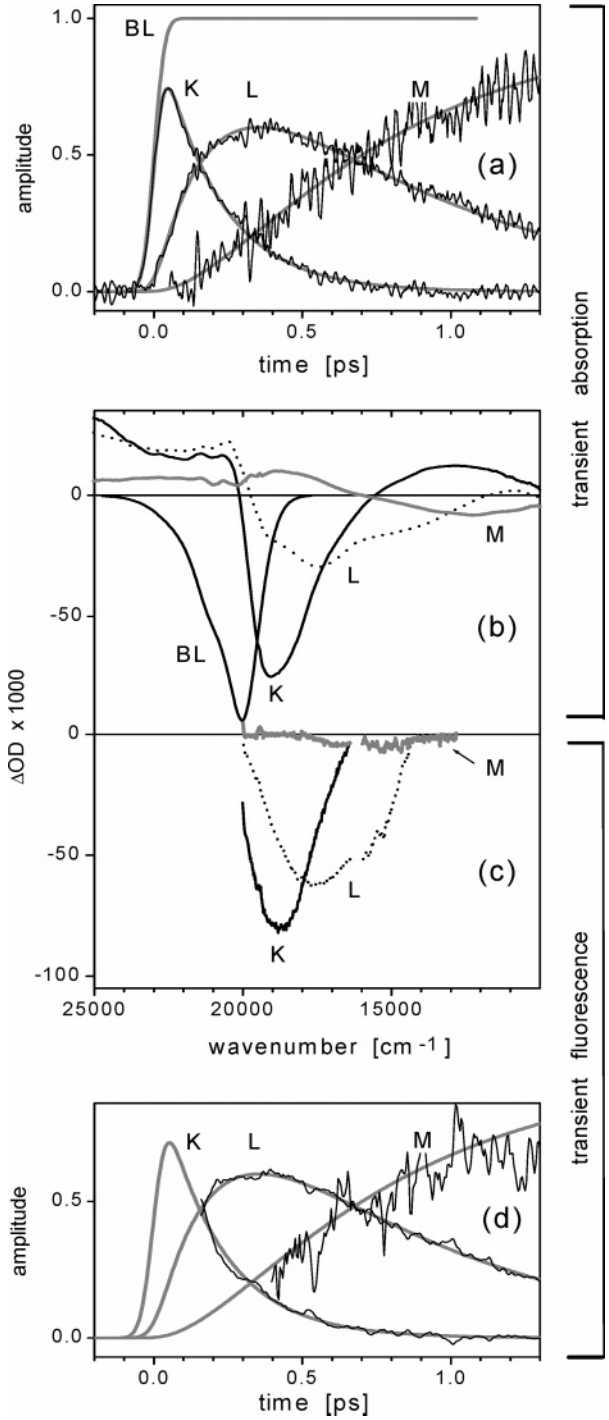

Figure 7. Joint decomposition of transient absorption and fluorescence spectra by global analysis. The evolution is described by a sequence K → L → M of virtual species in the excited state. Their relative populations are observed with different time-resolution in absorption (a) and emission (d). The associated spectra for the three states are shown in (b) and (c). Emission <14 000 cm^{-1} was not registered by time-resolved fluorescence for technical reasons. The associated spectra in (c) refer to stimulated emission rather than spontaneous fluorescence, to enable direct comparison with the absorption analogues in (b). Pump and probe polarizations were parallel for these measurements.

(Gaussian with 80 fs fwhm). The species-associated spectra are then expressed for stimulated emission, and in this way we obtain the characteristic "pure" SE spectra which are shown in Figure 7c. In this way the amplitudes in panels b and c were locked together.) The latter may be compared directly to the

(30) Ernsting, P. N.; Kovalenko, S. A.; Senyushkina, T.; Saam, J.; Farztdinov, V. *J. Phys. Chem. A* **2001**, *105*, 3443−3453.

corresponding SE components from transient absorption. Deep-red emission around 12 000 cm^{-1} was not observed by our time-resolved fluorescence experiment for technical reasons (vignetting in the spectrograph or input optics) even though the kinetics of spectral change toward the red can be extracted reliably from the fluorescence data.

The transient absorption measurements are examined next. For this purpose, we consider the initial period from −0.2 until 1.5 ps, which is largely shown in Figure 5a. The analysis proceeds in two stages. First, the induced spectra, including coherence, are decomposed into species-associated spectra as described in ref 30. The "species" in this case are the Gaussian pulse $G(t)$ which describes the coherent contribution[28] and the virtual states K, L, and M for the sequential contribution. (Time derivatives G', G'' were also included in the simulation of the coherent contribution.) The time constants k_1 and k_2 are taken from the previous section. This treatment provides mainly the time resolution (65 fs fwhm) of the measurement. The amplitude of the bleach component is determined from the transient spectrum at 1.5 ps. With this information, the bleach BL($\tilde{\nu}$,t) is simulated and subtracted from the data. The result is then re-analyzed in the second stage in order to obtain the ESA + SE spectra, which are shown in Figure 7b for the three states. The associated amplitudes or kinetic traces are presented in panel a. They represent the relative populations of K, L, and M as seen by transient absorption. Multiplying each of the traces with the corresponding spectrum (and the temporal traces $G(t)$, $G'(t)$, and $G''(t)$ with their associated spectra) and summing the result, we obtain the observed transient spectra of Figure 5a to within experimental noise of 0.6 mOD.

Let us compare the characteristic spectra for transient absorption (Figure 7b) and pure stimulated emission (Figure 7c). The initial band K looks almost identical in the two observation modes: the peak for stimulated emission (i.e., the most negative value) occurs around 19 000 cm^{-1}, and the shape mirrors the absorption spectrum quite well. (The peak from fluorescence upconversion occurs red-shifted by approximately 200 cm^{-1}, probably because of the inner filter effect from ground-state absorption.) From Figure 6, one finds that the fluorescence shifts to the red by 1000 cm^{-1} in 200 fs, and this observation is reflected in panel c by the second component L for pure stimulated emission, which has a broader peak at lower energy. (At 150 fs, the two are equally weighted (cf. Figure 5d), so that the corresponding Stokes shift is half of the peak separation.) Turning to transient absorption in panel b, the peak values for K and L are more separated compared to their counterparts in panel c. This difference is explained by excited-state absorption, which underlies transient absorption but does not contribute to fluorescence or pure stimulated emission derived from it. From a comparison, we conclude that excited-state absorption rises in a broad band from 15 000 to19 000 cm^{-1} with the (nominal) time constant $1/k_1 \approx 200$ fs. The observation of rising ESA in the bleach region of panel b, where SE is absent, supports this conclusion. The initial fluorescence occurs while the molecule twists away from the FC region, whereby radiative coupling to the ground state may diminish. When and at which emission frequency does this effect set in? To approach the problem consider the band integral

$$\mathrm{BI}_{\mathrm{fls}}(t) = \int \mathrm{FQD}(\tilde{\nu},t)/\tilde{\nu}^3 \mathrm{d}\tilde{\nu} \qquad (1)$$

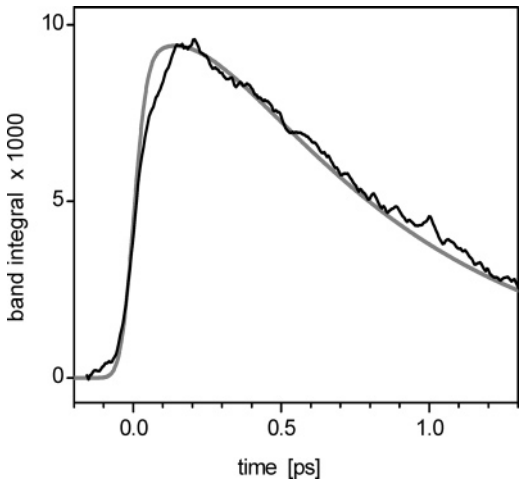

Figure 8. Band integral from femtosecond fluorescence spectra (Figure 6), which suggests that radiative S_1-S_0 coupling is constant for the initial 200 fs; see text. The result from global analysis for $t > 150$ fs is extrapolated to earlier time (gray curve).

which may be calculated directly from the femtosecond fluorescence spectra; the result (after normalization, the band integral for the pure stimulated emission spectrum K (Figure 5c) was set to that of the bleach BL (Figure 5b) so in this way, the amplitudes in panels b and c were locked together) is shown in Figure 8. If the population stays constant, $\mathrm{BI}_{\mathrm{fls}}$ is proportional to oscillator strength or the square of the $S_1 \rightarrow S_0$ transition dipole moment. Our experiment shows a *rise* of $\mathrm{BI}_{\mathrm{fls}}$, reaching a maximum at 150 fs, clearly slower than the integrated apparatus function which was obtained from upconverted Raman scattering. Since the population in S_1 can only decrease after the pump pulse is over, several cases should be considered: radiative coupling may *in*crease in the course of twisting or during brief nuclear coherence in another coordinate, or some artifact intervenes before 150 fs. The ambiguity can be reduced by the fluorescence analysis for $t \geq 150$ fs, which was summarized in Figure 7c,d. The band integrals are found to be nearly equal for the characteristic, empirical spectra K and L in Figure 7c. (In fact $\mathrm{BI}_K < \mathrm{BI}_L$ as observed, but spectrum K appears truncated at its blue side; equality should be achieved when the missing portion is reasonably appended.) It follows that radiative coupling $S_1 \rightarrow S_0$ does not decrease for 200 fs, during which time the FC region is vacated and characteristic spectra L are assumed. This conclusion is supported by the band integral for transient absorption further below.

A novel feature is presented by the broad SE band which is associated with transient state M. The band is directly observed by transient absorption (Figure 5a) since ΔOD is negative across the range of 10 000−18 000 cm^{-1} at 1 ps delay, for example. These measurements were often and well reproduced so that radiative coupling $S_1 \rightarrow S_0$ far below the initial emission frequency is certain. Long-lived fluorescence on a 4 ps time scale was also observed by upconversion. When the time constant $k_3 = 0.21$ ps^{-1} from transient absorption is used, a pure stimulated emission spectrum M is obtained, which is also shown in Figure 7c. Its blue flank matches the corresponding band in panel b quite well if allowance is made for underlying ESA. Below, we show that the deep-red emitting state M decays directly to the ground state so that no dark intermediate is populated on the S_1 energy surface; hence M can be identified with the minimum energy configuration there or with a wide

region close to a conical intersection.[19] The oscillator strength for stimulated emission M → S_0 can be estimated if the corresponding band is known completely. In Figure 7b, the transient absorption spectrum associated with M was shown, which consists of the SE and ESA contributions. Clearly, the part of the spectrum where ΔOD <0 is due to stimulated emission. If the integral is performed over this part only, one obtains a lower estimate of the oscillator strength, 20% relative to that of the BL band. More reasonable (but not certain) is the assumption that the ESA background extends linearly from its maximum around 19 000 cm^{-1} to zero at 10 000 cm^{-1}. In this case, the relative oscillator strength becomes 48%. We mentioned before that a conical intersection would be accidental with TO, which is why M probably corresponds to the global S_1 minimum. In this case the structure is essentially perpendicular and radiative coupling to the ground state should be significantly smaller than is actually observed. The observation therefore suggests that M is not perpendicular but instead represents a nonstationary, partly twisted region on the S_1 surface from where a conical intersection is accessed. The assignment should be decided by quantum-chemical calculations.

The emission time must be determined by spectrally averaging over the fluorescence decay. When the emission shifts to near-infrared during the decay, late portions may be missed by conventional quantum yield or time-correlated photon-counting measurements. Likewise, our fluorescence upconversion measurements were not sufficiently sensitive for $\tilde{\nu}$ < 14 000 cm^{-1}. Therefore, we turn to transient absorption because only this method could monitor the deep-red region. Under these conditions, SE + ESA are inseparable, and we treat all spectral change together by forming the band integral

$$\mathrm{BI}_{\mathrm{abs}}(t) \equiv \int \Delta\mathrm{OD}(\tilde{\nu},t)/\tilde{\nu}\, \mathrm{d}\tilde{\nu} \qquad (2)$$

over the full observation range, that is, the (relative) induced oscillator strength. Solvation may shift ESA or SE bands within the range but should not affect the full integral. One finds

$$\mathrm{BI}_{\mathrm{abs}}(t) \propto n_1(t)\,[-f_{\mathrm{abs}} - f_{\mathrm{SE}}(t) + f_{\mathrm{ESA}}(t)] \qquad (3)$$

The time dependence of oscillator strengths $f_{\mathrm{SE}}(t)$ and $f_{\mathrm{ESA}}(t)$ indicates electronic change, for example, while twisting around a central bond or along torsional motion of the thiazolyl moiety, and $n_1(t)$ is the population in the S_1 state. The full integral, which is shown in Figure 9a, can therefore be considered as a measure of electronic change through optical excitation, weighted by population. By 15 ps it has returned to zero (a small deviation is attributed to the limited integration range) indicating complete ground-state recovery. The inset shows the initial period on an expanded time scale. Immediately after excitation, the full absorption integral stays constant until 0.4 ps while the spectral change is substantial during this time (cf. Figure 5). An effective lifetime can be estimated as

$$\tau_{\mathrm{eff}} = \int \mathrm{BI}_{\mathrm{abs}}(t)\, \mathrm{d}t/\mathrm{BI}_{\mathrm{abs}}(0) = 4.7 \pm 0.1\ \mathrm{ps} \qquad (4)$$

with extrapolated $\mathrm{BI}_{\mathrm{abs}}(t \to 0)$ for normalization, and the inferred quantum yield becomes $\tau_{\mathrm{eff}}/\tau_{\mathrm{rad}} = (7.6 \pm 0.4) \times 10^{-4}$. (By stationary fluorescence, we measure a quantum yield of 1.2×10^{-4} for TO in methanol. This value presents a lower limit because emission <13 000 cm^{-1} was not registered; see Figure

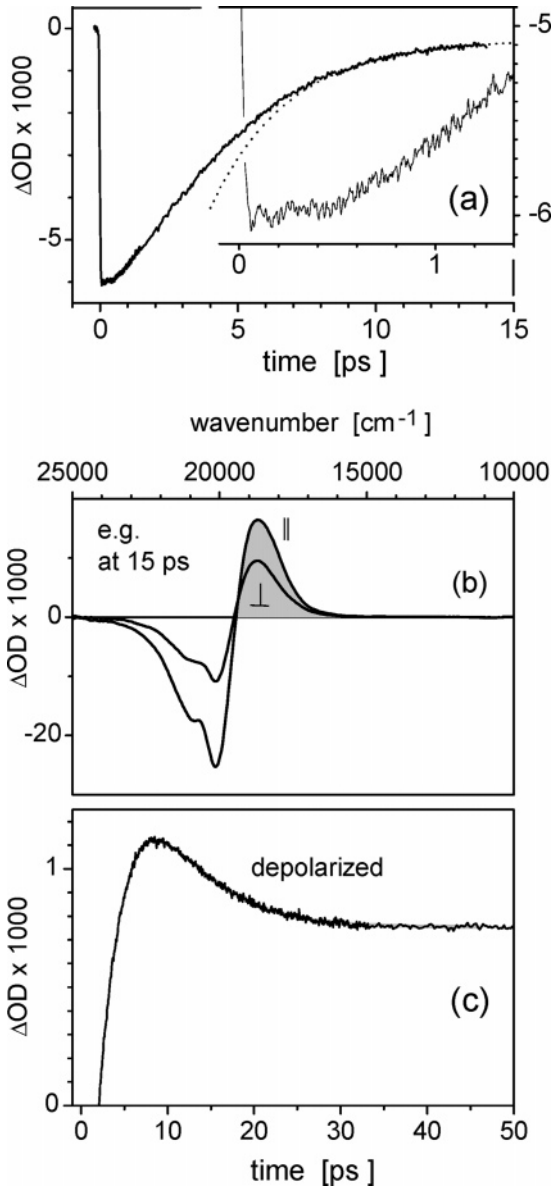

Figure 9. Picosecond dynamics of TO in methanol. (a) The full oscillator strength or band integral $\int\Delta\mathrm{OD}(\tilde{\nu},t)/\tilde{\nu}\, \mathrm{d}\tilde{\nu}$ monitors electronic change. Initially constant (cf. inset), the effective decay time shortens to 2.8 ps late in S_1 (dotted exponential curve). Data refer to magic-angle detection. (b) Hot ground-state molecules/photoisomers are responsible for a dispersive shape of the transient spectrum when $t \geq 15$ ps, for example, at $t = 15$ ps shown here for parallel and perpendicular polarizations. The partial band integrals from the lobes at lower energy (gray) are averaged to form the depolarized partial band integral (c). The latter measures the red-shift of the recovered ground-state absorption. It decays (time constant 4.6 ps) due to cooling and settles to a quasi-stationary value due to photoisomers.

1.) At late time in the S_1 state, the effective lifetime shortens to 2.8 ps (dotted line in Figure 9a). This type of nonexponentiality (if attributed to $n_1(t)$) is a hall-mark of diffusional motion of the torsional coordinate toward a conversion funnel.[31]

In summary, so far, the emission band mirrors the narrow absorption spectrum immediately after excitation and then experiences a dynamic Stokes shift of ∼1000 cm^{-1} and broadening in the initial 0.2 ps period. The radiative rate does not change significantly over this time. This phase appears to be similar to the relaxation to a shallow S_1 minimum which

(31) Bagchi, B.; Fleming, G. R.; Oxtoby, D. W. *J. Chem. Phys.* **1983**, *78*, 7375−7385.

was calculated for symmetrical thiacarbocyanine.[20] The emission band shape in the intermediate time range is particularly interesting because model calculations predict asymmetric stretching activity[18,20] after the FC region has been left (during process 2 in Figure 2). Correspondingly, one expects vibronic structure of the emission around 0.3 ps, where the contribution by virtual species L is largest. Referring to Figure 7, we indeed find vibronic structure for L, albeit with transient absorption only (panel b) because fluorescence upconversion did not extend sufficiently to the red (panel c). The L absorption spectrum is negative in the fluorescence range so that stimulated emission dominates here, and its structure may be considered reliable in view of the quality and reproducibility of the measurement. Simulations of the band shape with Brownian oscillators[25] suggest a dimensionless displacement $d \approx 1.8$, but systematic deviation remains for large Stokes shifts, that is, for higher members, $k'' \geq 3$, of the vibrational progression, $0' \rightarrow k''$. The deviation may be caused by (i) excited-state absorption which contributes to the transient absorption spectrum, and (ii) the effect of torsional distribution in S_1 and the corresponding spectral convolution with the S_1-S_0 energy gap. Both complications were neglected in the simulations; we estimate that neglect of (ii) is the more serious of the two. Support for the existence of vibronic structure may be drawn from the emission in ssPNA, which was shown in Figure 4—assuming that only intermediate twist angles are populated in this case. The transient absorption spectrum L is also represented in the figure (dotted line); note that direct comparison suffers equally from unknown (i) and—to a lesser extent—from unknown (ii). On balance, we conclude that TO emission in methanol exhibits high-frequency vibrational structure in the intermediate time range. The dynamic Stokes shift continues and slows gradually until, by about 2 ps, a broad quasi-stationary emission band is reached which is centered around 12 000 cm^{-1} and extends below 10 000 cm^{-1}. From here, internal conversion takes place, and the remainder deals with processes in the ground state. The following is therefore not relevant to the theme and title of the paper, but it closes the photochemical cycle of TO and, from a methodical point of view, shows further possibilities of band integrals for condensed-phase spectroscopy.

The partial band integral is taken from dispersive $\Delta OD(\tilde{\nu},t)$, which dominates from 10 ps onward, by integrating $\Delta OD(\tilde{\nu},t)$ over the red lobe only (Figure 9b). It is a measure of broadening on the red flank of the recovered ground-state absorption, either because the molecular temperature has increased or because a photoisomer was created with a red-shifted absorption spectrum. The result is shown in Figure 9c. The relaxation immediately after 10 ps is best described by 4.7 ps rise from internal conversion together with 4.6 ps exponential decay. The latter time constant is of the same order as that found for cooling of *p*-nitroaniline in methanol[32] and is therefore ascribed to the same process. The remaining oscillator strength does not diminish until our last observation time of 125 ps; it should be due to the photoisomer. (The asymmetry of the partial band integrals decays with a time constant of 124 ps due to rotational diffusion of the photoisomer.) Referring to the scheme of intermediates, $X(S_0)$ and $Y(S_0)$ represent the hot and equilibrated photoisomer, respectively.

We conclude that a high-frequency mode (coordinate q) plays an important role in the structural reorganization of Thiazole Orange following $S_1 \leftarrow S_0$ optical excitation. The participation of another mode in the deactivation of cyanines has been described as a sequence of processes: fast vibrational relaxation followed by torsional motion.[33] By observing vibronic structure of stationary emission in polynucleotides and of femtosecond transient emission in methanol solution, we showed instead that the high-frequency mode appears during torsion, which is taken to be the primary dynamical variable (coordinate τ). The observations are in agreement with recent model calculations.[18−20] As the molecule twists away from the FC region, the mode becomes more displaced. In this way, better overlap between the lowest vibrational wave function, $\varphi_0^{S1}(q)$, in S_1 with higher wave functions, $\varphi_k^{S0}(q)$, in S_0 is achieved. Note that $\varphi_0^{S1}(q)$ depends on τ as a parameter. Good vibrational overlap between S_1 and S_0 is a general condition for nonadiabatic coupling to become effective between the two electronic states. Even if the coupling coordinate Q is different from q, increasing mode displacement along q during torsion in S_1 helps provide ever higher accepting levels in S_0, in combined radiationless transitions $\psi_i^{S1}(Q)\,\phi_0^{S1}(q) \rightarrow \psi_j^{S0}(Q)\,\phi_k^{S0}(q)$. In effect, the S_1-S_0 energy gap is reduced by the vibrational energy $E_k^{S0}(\tau)$. Fast twisting motion along τ is thus leveraged into an even faster-shrinking effective energy gap, and internal conversion ensues.

4. Experimental Section

4.1. Materials. The carboxy derivative of TO with R = HOOC−CH_2− was synthesized and purified as described.[34] The synthesis of peptide nucleic acids containing TO as a base (TO/PNA)[24] and their hybridization with complementary DNA strands was reported in refs 13 and 14. Stationary absorption and fluorescence measurements of TO/PNA and hybridized solutions were performed in a degassed pH 7.0 buffer (100 mM NaCl and 10 mM NaH_2PO_4). Hybridizations were done by heating TO/PNA and DNA (mixed 1:1) to 85 °C (5 °C/min) for 20 min followed by cooling to 25 °C (1 °C/min). The concentration of duplex solutions was 1.5 μM. All transient measurements were performed in methanol (Merck Uvasol) at ambient (~23 °C) temperature.

4.2. Stationary Measurements. Absorption spectra were measured with a Shimadzu UV310 spectrometer. The validity of the Lambert−Beer law was examined and found to be valid over the concentration range of 5.1×10^{-6} to 2.55×10^{-4} M in methanol. No systematic deviation could be detected. The presence of TO aggregates at the highest concentration used (see below) can therefore be excluded. Fluorescence spectra were recorded from dilute solutions with a modified Spex 212 fluorometer. Solvent background signal was subtracted, and photometric correction was achieved with reference dyes.[35] Quantum yield measurements were performed by comparison with emission from fluorescein (0.1 M NaOH).

4.3. Transient Absorption Spectroscopy.[36] Thiazole Orange in methanol was excited by 40 fs pulses centered at 484 nm (60 Hz). The pulse energy was typically 0.5 μJ on a spot of 150 μm diameter. The sample thickness was 0.35 mm, and the optical density was 0.65 at the absorption maximum corresponding to a concentration of 2.3×10^{-4} mol/L. The pump-induced transient absorption signal, $\Delta OD(t, \lambda)$, was

(32) Kovalenko, S. A.; Schanz, R.; Hennig, H.; Ernsting, N. P. *J. Chem. Phys.* **2001**, *115*, 3256−3273.
(33) Huang, Y.; Cheng, T.; Li, F.; Hunag, C.-H.; Wang, S.; Huang, W.; Gong, Q. *J. Phys. Chem. B* **2002**, *106*, 10041−10050.
(34) Deligeorgiev, G. T.; Gadjev, I. N.; Drexhage, H. K.; Sabnis, W. R. *Dyes and Pigments* **1995**, *29*, 315−322.
(35) Gardecki, J. A.; Maroncelli, M. *Appl. Spectrosc.* **1998**, *52*, 1179−1189.
(36) Kovalenko, S. A.; Dobryakov, A. L.; Ruthmann, J.; Ernsting, N. P. *Phys. Rev. A* **1999**, *59*, 2369−2384.

monitored by supercontinuum probe pulses covering the spectral range $340 \leq \lambda \leq 1000$ nm, through a prism spectrograph which provided a well-suited energy dispersion. Measurements from 50 shots were averaged, and the recorded spectra were time corrected for the chirp of the supercontinuum. The pump−probe intensity cross correlation measured over the probe region is described by a 65 fs (fwhm) Gaussian shape. Variations of the pump pulse energy in the range of 0.13−1.0 μJ had no effect on the transient spectral shapes.

4.4. Fluorescence Upconversion Spectroscopy.[29] The sample solution ($\sim 2 \times 10^{-4}$ mol/L, optical path = 0.40 mm) was excited by 40 fs, 0.5 μJ pulses at 450 nm (500 Hz). Fluorescence was imaged onto a thin (0.2 mm) KDP crystal by reflective spherical optics. Near-infrared gate pulses (40 fs, 1.30 μm, 60 μJ) were used for sum-frequency mixing with the entire fluorescence band. Background-free measurement with 80 fs time resolution (fwhm) was achieved in a noncollinear geometry with tilted fronts for the gate pulses. The upconverted signal was dispersed by a prism spectrograph and integrated (1 s) on a CCD camera. Photometric correction was effected by similar measurements with standard fluorescence dyes.

Acknowledgment. The authors thank D. V. Jarikote for providing samples, V. Fartzdinov for semiempirical calculations, and T. Werncke for valuable discussions. The work was supported by the Fonds der Chemischen Industrie, by the Volkswagen Foundation in the priority research area "*Intra- and Intermolecular Charge Transfer*", and by the Deutsche Forschungsgemeinschaft in the collaborative research program "*Analysis and Control of Fast Photoinduced Processes*".

JA056862N